Analysis of Dual Gate Structures Using Double-Well and WKB Quantization Rules

Amr M. Bayoumi, *Senior Member, IEEE*

***Abstract*— An alternative method for direct calculation of energy levels for symmetric dual gate structures with body widths of 3–10 nm is presented in the current paper, using double well analysis and Wentzel-Kramers-Brillouin (WKB) quantization rules. The double well analysis explains the lower energy level splitting, as well as the twin shape of the corresponding wave function with odd–even symmetry. The potential is approximated using a parabolic potential. The perturbation analysis, which already gives good accuracy for higher energies and lower electron effective mass, is compared with the current approach. The combination of the double well and WKB method gives improved accuracy for energies below barrier maximum potential, over perturbation potential, while a simple analytic second-order WKB correction term is needed for energies just above the potential peak. Using the WKB representation of wave function, the effect of finite barrier height on wave function penetration and on energy levels is analytically treated, for all energy levels, with barriers as low as 0.5 eV. Theoretical models are verified using numerical eigenvalue/eigenvector solvers, while device modeling results are compared with self-consistent simulator.**

***Index Terms*— Double-well, dual gate (DG), quantum mechanical effects, wave function penetration, Wentzel-Kramers-Brillouin.**

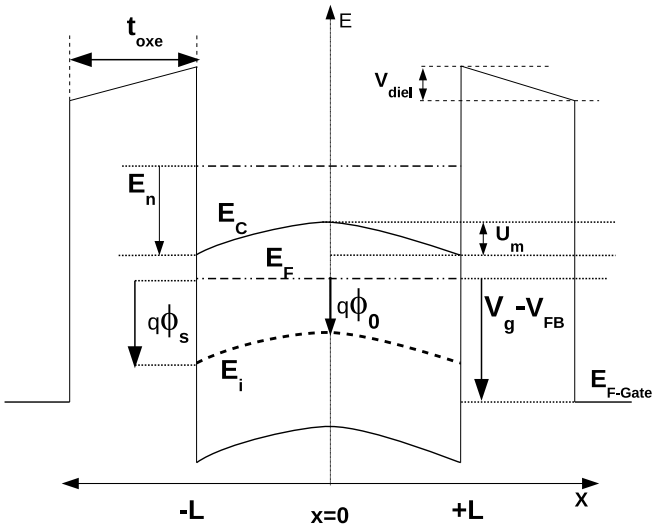

Fig. 1. Band diagram for a DG structure.

I. Introduction

THIS paper focuses on symmetric dual gate (SDG), where 1-D analysis of the DGs is used as a cornerstone for FinFET modeling. In these structures, the high-k gate dielectric stack has an equivalent oxide thickness below 1 nm, while the body thickness ranges between 3–10 nm, with low-moderate doping, and metal gates with workfunctions close to mid-gap [1]. This forms a quantum well with discrete energy levels.

Fig. 1 shows a 1-D representation of potentials in a cross section of a SDG structure. DG structures were studied classically to understand the basic device behavior such as central and surface potential concepts [2], [3]. Quantum mechanical treatment was adopted in [4] to account for both structural confinement between the two walls of the fin, and electronic confinement within the potential well inside the silicon body. However, it used the variational approach using a trial wave function, required a guess for several bias-controlled parameters, and assumed only the first level occupancy for potential development.

Manuscript received February 16, 2016; revised May 27, 2016; accepted June 27, 2016. Date of publication July 27, 2016; date of current version August 19, 2016. The review of this paper was arranged by Editor J. Knoch.

The author is with the Department of Electronics and Communications Engineering, Arab Academy for Science and Technology, P.O. Box 2033-Elhorria, Heliopolis, Cairo, Egypt (e-mail: amr.bayoumi@aast.edu).

Color versions of one or more of the figures in this paper are available online at http://ieeexplore.ieee.org.

Digital Object Identifier 10.1109/TED.2016.2587882

The perturbation-based approach, which assumes that a potential perturbation is applied to a 1-D infinite potential well, has been used in several reports. Some authors have developed analytical techniques for low effective mass cases, where the structural confinement dominates [5], [6], and used this as a starting point to arrive to an initial form of the wave function. Then, the resulting electron distribution was used to solve Poisson's equation in order to calculate a potential perturbation to the initial box potential. However, they made a prior assumption of the wave function as a sinusoid, corresponding to the classic particle-in-a-box with flat zero-potential in the well. Electron occupancy was also limited to the ground level in their calculation of perturbation potential. This could be justified for the materials they analyzed with very low effective mass of $\sim$0.05 m_o, which is much smaller than that of silicon, which falls between 0.19 m_o and 0.916 m_o.

A parabolic potential perturbation has also been assumed in [7]–[9]. This however does not account for the fact that the first level(s) can be in some cases dominated by electronic confinement, with minor effect from the box-like structural confinement, and that the non-perturbed energy could be smaller in magnitude than the resulting change in energy, or than the perturbing potential. As will be shown, it sometimes shows errors as large as 10%–20% for the first energy level(s), or can even give misleading results for wider body thicknesses. This technique works best when the well is very thin or when the energy level is higher than potential perturbation, such as for low effective mass cases. Still, the concept of a parabolic well potential is adopted in this paper, as will be discussed.

The Wentzel-Kramers-Brillouin (WKB) approximation and its associated quantization rules can be used to analytically calculate energy levels and wave functions, given a known potential well shape [10], [11]. This method mainly depends on the potential distribution, and does not require any prior knowledge of the wave function or energy levels. It can also be used to analytically express the wave function. It has its own limitations as well, when the energy levels are close to the potential, where the momentum approaches zero. The work reported in [12] uses the WKB technique to calculate the energy levels in SDG and asymmetric DG structures, but still needs the Newton–Raphson method to solve a nonlinear equation at each energy level. It also does not consider the interaction of electron wave functions for energies below the maximum of the central potential U_m at $x = 0$, as will be shown shortly.

Independent of the approaches used to calculate the energy levels; the above-mentioned reports do not treat the lower energy levels dominated by electronic confinement as double wells. The electrons confined in these two wells interact through tunneling, resulting in a energy level splitting [13]–[15]. This is a well-known problem in physics and chemistry, where, for example, the potentials due to the interaction of two similar atoms in a molecule result in the energy level splitting. The main idea is to first isolate each well (without changing the potential distribution), and calculate the energy levels before bringing them close, followed by a calculation of the energy splitting. The WKB method is most suitable for finding these isolated energies, since it is not affected by the boundary conditions at the other potential wall beyond the turning points. The WKB technique is thus explored in this paper, in combination with double well analysis.

It is worthwhile noting that the application of quantization rules directly to double wells with four turning points have been also considered [17], [18]. However, the solution is mathematically more complex. The current approach has the advantage of explaining the physics of the energy level splitting from the different view of interaction between wells.

The WKB rules require prior knowledge of the spatial distribution of the potential. For devices with gate voltages of less than 1 V, and body thicknesses of the order of 5–10 nm, the fitting of the potential to a parabolic model of potential for a SDG structure was demonstrated [7]–[9], [12]. This behavior is verified using self-consistent simulations in the current work, and is used as a demonstration tool.

Metal/high-k dielectrics gate-stacks for DG FETs are predicted to have equivalent oxide thickness, $t_{\rm oxe}$, of down to 0.5 nm, and operating voltages of 0.6–0.9 V, with $W_{\rm fin}$ less than 5 nm [1]. Thus, wave function penetration takes place, and affects the energy levels [19], [20]. Some reports modeled these changes in ground energy levels only [5], [6], and under the assumption of a predetermined sinusoidal wave function. In addition, the phase angles that can be used to reproduce the wave function analytically under these penetration conditions are not analytically expressed. This will be analyzed in the current work, for all energy levels and dielectric barriers as low as 0.5 eV.

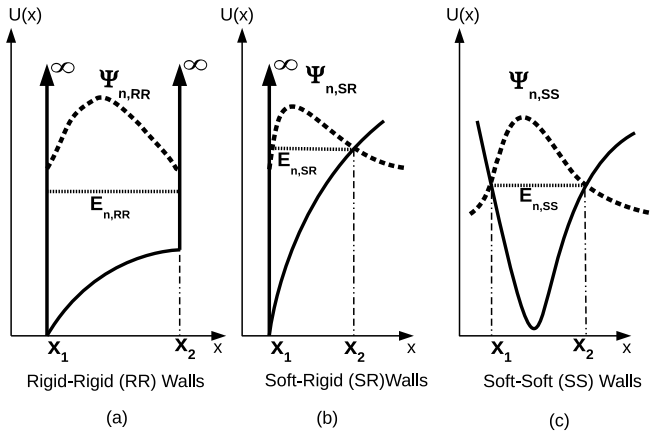

Fig. 2. Potential wells used in WKB selection rules. x_1 and x_2 represent the classical turning points. (a) RR walls. (b) SR walls. (c) Soft–soft walls.

Widely adopted eigenvalue/eigenvector solvers [21] are used to verify the theoretical steps and calculations. Self-consistent device simulators [22], [23] are used to verify the device-related model.

II. Theoretical Background

A. WKB Selection Rules

The treatment in section follows [10]. Fig. 2 shows the potential wells used in the analysis. An electron with an energy E_n, corresponding to level n, in a well with potential $U(x)$, will have a momentum $p_n(x)$ defined as

$$p_n(x) = \sqrt{2m_j[E_n - U(x)]} \tag{1}$$

where m_j is the effective mass in the jth well. The WKB representation of wave function $\psi_n(x)$ near the left-hand side turning point x_1 inside a potential well, where $E_n > U(x)$, using an angle $\theta_n(x)$

$$\begin{aligned}\psi_n(x) &= \frac{A_1}{\sqrt{p_n(x)}}\sin(\theta_n(x)) \\ &= \frac{A_1}{\sqrt{p_n(x)}}\sin\left(\frac{1}{\hbar}\int_{x1}^{x} p_n(x)dx\right).\end{aligned} \tag{2}$$

In the classically forbidden region, $\psi_n(x)$ becomes

$$\psi_n(x) = \frac{B_1}{\sqrt{|p_n(x)|}}\exp\left(\frac{-1}{\hbar}\int_{x}^{x1} |p_n(x)|dx\right) \tag{3}$$

where A_1 and B_1 are the normalization coefficients. For rigid–rigid (RR) walls, with both being infinite, the following rule applies:

$$\theta_{n,\rm RR} = \frac{1}{\hbar}\int_{x1}^{x2} p_n(x)dx = (n+1)\pi, \quad n = 0, 1, 2, \ldots \tag{4}$$

For the soft-rigid (SR) walls, when one potential wall is infinite, while the other is soft, θ is expressed as

$$\theta_{n,\rm SR} = \frac{1}{\hbar}\int_{x1}^{x2} p_n(x)dx = (n+3/4)\pi. \tag{5}$$

These are known as the WKB quantization rules [10], [11].

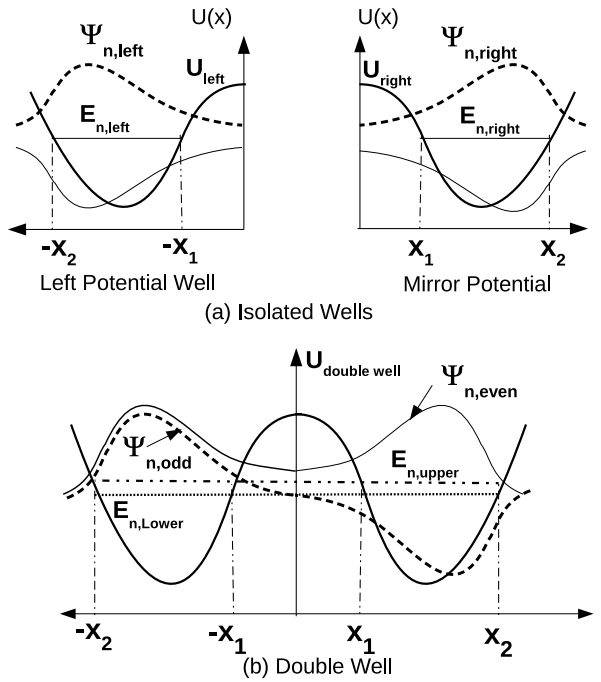

Fig. 3. (a) Two identical isolated mirror wells. (b) Double well formed after bringing them close. For double well analysis in this paper, it is assumed that the isolated potentials do not change after interaction.

B. Double-Well Analysis

The double-well wave function analysis is summarized in next paragraphs. A detailed treatment can be found in either [14] or [16]. Fig. 3 Shows the basic elements used in the analysis. First, the two wells are assumed to be independent, with each having energy level E_n^0, and wave function Ψ_n^0. The superscript *0* represents the isolated well case. The isolated potential profiles are assumed to be in their final form, i.e., they will not change after interaction. The isolated energies are calculated by solving the energy levels for the potential of half the structure, using the WKB quantization rules. This is because the WKB rules require knowing the boundary conditions only at the classical turning points (x_1 and x_2).

The origin of the double well interaction comes from the finite probability of tunneling between the two wells through the middle barrier. The superposition of the two originally-isolated wave functions results in a system with new two wave functions with: 1) even symmetry, where addition takes place and 2) odd (or anti) symmetry, where the wave functions are subtracted from each other. This is represented as

$$\psi_{n,\text{Double Well}} = \frac{1}{\sqrt{2}}\left[\psi^0_{n,\text{Left}} \pm \psi^0_{n,\text{Right}}\right]. \tag{6}$$

This explains the twin wave function shape with odd–even symmetry for the first two energy levels in the DG structures (or any energy level lower than middle barrier height).

Solving two new wave functions will result in two eigen energies. This is mathematically equivalent to the splitting the original energy level with equal energy offset ΔE_n. The new energies become

$$E_{n,\text{Double Well}} = E_n^0 \pm \Delta E_n \tag{7}$$

where the $-$ve term corresponds to the even symmetry wave function. The energy split term ΔE_n can be calculated as

$$\Delta E_n = \frac{1}{2d\theta_n^0/dE}\exp\left(-\frac{1}{\hbar}\int_{-x1}^{x1}\left|p_n^0(x)\right|dx\right) \tag{8}$$

where p_n^0 is the electron momentum in the isolated well corresponding to the energy level E_n^0. The derivative term in (8) is the differentiation of (5) with respect to energy, calculated as

$$d\theta_n^0/dE = \frac{1}{\hbar}\int_{x1}^{x2}\frac{m_j^{1/2}}{\sqrt{2\left[E_n^0 - U(x)\right]}}dx. \tag{9}$$

C. Perturbation Technique for DG Wells

The parabolic perturbation approach, assumes a parabolic potential perturbation is applied to a box-like 1-D infinite potential well [7]–[9]. The energy levels are expressed as

$$E_{\text{pert}} = \frac{(n+1)^2\pi^2\hbar^2}{2m_j(2L)^2} + 2U_m\left[\frac{1}{\pi^2(n+1)^2} + \frac{1}{3}\right] \tag{10}$$

where the first term in the right hand side is the unperturbed energy level corresponding to particle-in-a-box, while the second term represents the perturbation.

III. Potential in Ultrathin DG

Of practical importance, are the ultrathin SDG structures with body thickness of less than 10 nm [1]. In this thickness regime, it was shown that the potential can be fitted to a parabolic model [7]–[9]. Therefore, the parabolic potential is used as a starting point.

Fig. 1 shows the band diagram for the DG structures. For DG device calculations, the potential $\varphi(x)$ represents the separation of the intrinsic potential from Fermi level. Using a parabolic well formula between $x = -L$ and $x = +L$, where $L = W_{\text{fin}}/2$, the potential can be expressed as

$$\begin{aligned}\phi(x) &= \phi_0 + (\gamma/2q)x^2 \\ \gamma &= 2q(\phi_s - \phi_0)/L^2 = 2U_m/L^2\end{aligned} \tag{11}$$

where φ_0 and φ_s are the potentials at $x = 0$ and $\pm L$, respectively, $U_m = q(\varphi_s - \varphi_0)$ is in eV, while q is the electron charge. At the surface, at $x = -L$

$$\frac{d\phi(-L)}{dx} = -\gamma L = \frac{-\epsilon_{\text{ox}}}{\epsilon_{\text{Si}}}(V_g - V_{\text{fb}} - \phi_s)/t_{\text{oxe}} \tag{12}$$

where ε_{oxe} and ε_{Si} are the permittivities of the equivalent SiO_2 thickness and silicon, while V_g and V_{FB} are the applied gate voltage and the flatband voltages, respectively. Combining (11) and (12) results in an expression for φ_s as a function of φ_o and the known device parameters

$$\phi_s = \frac{1}{1 + \epsilon_{\text{ox}}L/(2q\epsilon_{\text{Si}}t_{\text{oxe}})}\left[\phi_0 + \frac{\epsilon_{\text{ox}}L}{2q\epsilon_{\text{Si}}t_{\text{oxe}}}(V_g - V_{\text{fb}})\right]. \tag{13}$$

Here, φ_0 can be approximated using the formulas in [9] and [25], for room temperature and intrinsic doping.

Fig. 4 compares the representative potential distributions using the model equations (11) and (13), with self-consistent device simulations for the cases of: 1) $W_{\text{fin}} = 5$ nm,

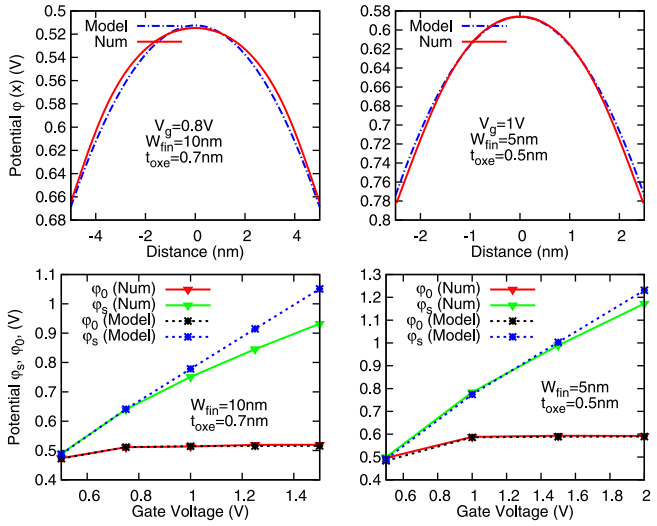

Fig. 4. Top: potential distribution in an SDG structure using current model and SCHRED simulator. Bottom: variation of potential at surface (φ_s) and midpoint (φ_o) with gate voltage V_g. For $V_g < 1$ V, intrinsic doping and room temperature are assumed. φ_o is calculated using the formulas in [9] and [25].

$t_{\text{oxe}} = 0.5$ nm, and $V_g = 1$ V, and 2) for the more practical International Technology Roadmap for Semiconductors (ITRS)-predicted case of $W_{\text{fin}} = 10$ nm, $t_{\text{oxe}} = 0.7$ nm, and $V_g = 0.8$ V. Fig. 4 also compares the model for the surface and midpoint potentials dependence on gate voltages. For body thickness less than 10 nm and t_{oxe} of less than 1 nm, the model gives reasonable prediction of ψ_s and ψ_0 for $V_g < 1$ V, which is higher than the maximum supply voltage of 0.6–0.9 V predicted for these technologies by the ITRS (i.e., $V_g = 1$ V is the voltage enough to drive the structure into strong inversion) [1]. For higher gate voltages, or for a silicon body thickness range of 15–20 nm, some deviation takes place from the parabolic potential model as the central potential tends to be flat. This is a result of less interaction between the two gates, due to the large separation (i.e., wide fins), and/or screening effects by inversion charges at high V_g.

IV. Energy Levels for Parabolic Potential in SDG

For the purpose of quantum well analysis, the potential minimum is placed at 0 eV, while the maximum U_m is at $x = 0$. $U(x)$ needs to be offset accordingly as

$$U(x) = q(\phi_s - \phi_0) - (\gamma/2)x^2 = U_m - (\gamma/2)x^2. \quad (14)$$

A. Double-Wells ($E_n < U_m$)

1) Isolated Parabolic Well Using WKB Rigid-Soft Rules: At the classical turning point $\pm x_0$, E_n is equal to $U(\pm x_0)$. Using (14), the isolated energy level E_n^0 can be expressed as

$$E_n^0 = U(\pm x_{0n}) = U_m - (\gamma/2)x_{0n}^2. \quad (15)$$

The expression for momentum in (1) then becomes

$$p_n(x) = \sqrt{m_j\gamma\left[x^2 - x_0^2\right]}. \quad (16)$$

This well is made of a hard potential wall at the semiconductor–dielectric interface, and a soft wall at the parabolic potential inside the semiconductor. Defining β_1 as

$$\beta_1 = (n + 3/4)\pi\hbar/\sqrt{m_j\gamma}. \quad (17)$$

The quantization rules for rigid-soft well are applied, where the integral in (9) can be evaluated as [26]

$$I_1 = \beta_1 = \int_{-L}^{-xo}\sqrt{x^2 - x_0^2}dx = \frac{L}{2}\sqrt{L^2 - x_0^2} + \frac{x_0^2}{2}\alpha$$
$$\alpha = \ln\left|-L/x_0 + \sqrt{L^2/x_0^2 - 1}\right|. \quad (18)$$

The logarithmic term α needs to be further simplified. An initial guess for x_o can be made using the triangular well approximation. By assuming a linear potential

$$U_{\text{linear}} = U_m - (U_m/L)|x| \quad (19)$$

the extrapolated $x_{o,\text{linear}}$ becomes

$$x_{o,\text{linear}} = \frac{L}{U_m}E_{n,\text{linear}} = \frac{L}{U_o}\left[\frac{3L}{4U_o}\frac{(n + 3/4)h}{\sqrt{2m_j}}\right]^{2/3}. \quad (20)$$

Substituting this value of $x_{o,\text{linear}}$ in α results in α_{linear}. Rearranging (18) gives a polynomial

$$\alpha_{n,\text{linear}}^2 x_{0,n}^4 - [4\beta_1\alpha_{n,\text{linear}} - L^2]x_{0,n}^2 + 4\beta_1^2 - L^4 = 0. \quad (21)$$

Solving for $x_{0,n}^2$ to get the energy level E_n^0 of an individual isolated well and substituting in (15)

$$E_{n,\text{SR}}^0 = U_m - \frac{\gamma}{4\alpha_{n,\text{linear}}^2}\Big[\left(4\beta_1\alpha_{n,\text{linear}} - L^2\right) + \sqrt{\left(4\beta_1\alpha_{n,\text{linear}} - L^2\right)^2 - 4\alpha_{n,\text{linear}}^2\left(4\beta_1^2 - L^4\right)}\Big]. \quad (22)$$

Equation (22) gives an error of less than 1%–5%. Using $x_{o,n}$ from (22) in (11) to replace the linear guess $x_{o,\text{linear}}$, followed by using the new result of alpha in (22) one more time typically reduces the error down to less than 1–3 mV.

2) Double-Well Energy Splitting: Next, the energy splitting is calculated using (8) and (9). The integral in (8) is a standard problem in tunneling through a parabolic barrier [16] and can be evaluated as

$$\Delta E_n = \frac{1}{2d\theta_n^0/dE}\exp\left[-\pi x_{0,n}^2\sqrt{m_j\gamma}/(2\hbar)\right]. \quad (23)$$

The derivative term of (9) can be evaluated using integration from $-L$ to $-x_0$ (or $+x_0$ to $+L$) to get

$$d\theta_n^0/dE = \frac{\sqrt{m_j/\gamma}}{\hbar}\ln\left|L/x_{0,n} + \sqrt{L^2/x_{0,n}^2 - 1}\right| \quad (24)$$

$E_n^{\pm}$ is calculated using (7).

Table I shows the example energy splittings for several values of W_{fin} and U_m, where the numerical results using eigenvalue solver is compared with the model equations. It also shows that the perturbation technique for energies below U_m can occasionally introduce substantial errors or even totally fail. From a mathematical point of view, the crossing of the $n = 0$ energy level using (10) to become higher than that for $n = 1$ is a result of the particle-in-a-box term having an $(n + 1)^2$ dependence, being added to the perturbation term with $1/(n+1)^2$ dependence. For wider fins or heavier effective mass, the particle-in-a-box term is multiplied by a factor of $1/L^2 m_{\text{eff}}$, and becomes less important.

TABLE I
EXAMPLE OF ENERGY SPLITTING RESULTS ($m_{\text{eff}} = 0.916$ M$_o$)

W_{fin} nm	Method	U_m meV	Isolated Energy, E_{n0} meV	ΔEn meV	E- meV	E+ meV
5	Eigen Solver	200		10.77	179.9	201.47
	Double-Well + WKB		189.3	10.77	177.8	199.4
	Perturbation			9.49	189.4	208.48
8	Eigen Solver			1.88	107.39	111.16
	Double-Well + WKB	130	109.4	2.016	107.42	111.46
	Perturbation			*-0.26*	*119.42*	*118.9*
10	Eigen Solver	150		0.191	107.9	108.3
	Double-Well + WKB		108.5	0.203	108.3	108.7
	Perturbation			*-5.25*	*134.5*	*124.0*

The derivations for parabolic perturbation in [7]–[9] assume that the wave function used to calculate the perturbed Hamiltonian is a pure sinusoid (half-wave for $n = 0$, and one fullwave for $n = 1$). This is clearly different from the actual odd–even symmetric wave function pairs expressed in (6) for $E_n < U_m$. Another issue is the fact that for wider wells and heavier effective mass, the unperturbed energy itself could be much smaller than U_m driving the perturbation potential. For example, at $U_m = 0.2$ eV, $W_{\text{fin}} = 10$ nm, and $m_{\text{Si}} = 0.916$ m$_o$, the box-like unperturbed energy term is 4.1 and 16.4 meV for $n = 0$ and 1, respectively. The corresponding perturbation terms in (10) are 130.4 and 107.6 meV. In this case, the validity of the first-order perturbation might need to be reconsidered.

B. Higher Energy Levels in Rigid–Rigid Well (En > Um)

The RR quantization rules in (4) can be rewritten as

$$I_2 = \int_{-L}^{L} \sqrt{(E_n - U_m) + (\gamma/2)x^2}\,dx = \beta_2$$
$$\beta_2 = (\hbar/\sqrt{2m_j})[(n+1)\pi + \sigma_{\text{corr,RR}}]. \tag{25}$$

A small second-order correction term, σ_{corr}, to the WKB integral is introduced, which helps improving results for light effective masses when E_n is close to U_m [24]. A treatment to arrive to a simple closed form is presented in the Appendix. The integral I_2 can be evaluated to yield a second-order equation in $E_n - U_0$, which can be solved as

$$E_{n,\text{RR}} = U_m + \frac{\gamma}{F_2^2}\left\{\left[\frac{F_2\beta_2}{\sqrt{\gamma/2}} - L^2\right] - \sqrt{\left(\frac{F_2\beta_2}{\sqrt{\gamma/2}} - L^2\right)^2 - \frac{2F_2^2}{\gamma}\left(\beta_2^2 - \frac{\gamma}{2}L^4\right)}\right\} \tag{26}$$

where

$$F_2 = \ln\left|\frac{1+\sqrt{E_n/U_m}}{1-\sqrt{E_n/U_m}}\right| \tag{27}$$

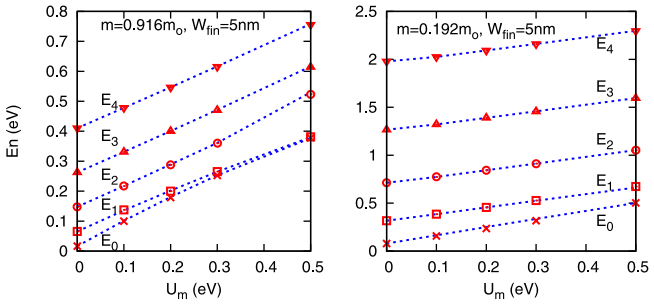

Fig. 5. Dependence of energy levels (E_0–E_4), for $W_{\text{fin}} = 5$ nm, on maximum potential at center U_m, for infinite barriers, and ideal parabolic potential. The x-axis at $U_m = 0$ represents the ideal particle-in-box potential. The symbols represent the numerical eigenvalue solver results, while lines represent the model.

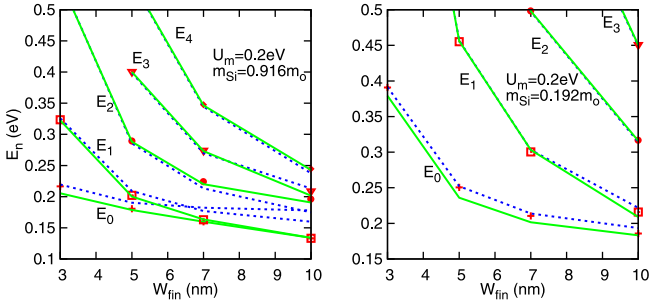

Fig. 6. Comparison of energy level dependence on fin width for both the perturbation (dashed lines) and WKB (solid lines) approaches, with the numerical eigenvalue results (symbols). U_m is fixed at 0.2 eV.

F_2 is approximated using an initial guess of E_n, such as the quadratic perturbation approach in (10), known to work well for higher energies [7]–[9].

C. Model Accuracy

Fig. 5 shows the model results of E_n for $W_{\text{fin}} = 5$ nm, as a function of maximum potential U_m, for both $m_{\text{Si}} = 0.916$ m$_o$ and 0.19 m$_o$, which represent the two possible extremes for Si. It is clear that the assumption of a flat zero potential (equivalent in Fig. 5 to $U_m = 0$) is not acceptable for devices in inversion.

As discussed earlier, the WKB approach can give improvements over the perturbation technique for energies below U_m. This is shown in Fig. 6, where the perturbation approach can give misleading results, for example, for the two lowest energy levels at $W_{\text{fin}} > 7$ nm, $m_{\text{Si}} = 0.916$ m$_o$, and $E_n < U_m$.

The errors using the WKB method are more pronounced for lighter effective mass and narrower well, when the separation of energy level from the potential peak becomes small. The WKB approximation requires that $\hbar|p'(x)| \ll [p(x)]^2$ [10], [11]. For parabolic potential, with $E_n > U(x)$, and using $\gamma = 2U_m/L^2$, this becomes

$$E_n - U(x) \gg \frac{[2\hbar U_m x]^{2/3}}{2L^{4/3}m_{\text{Si}}^{1/3}}. \tag{28}$$

This shows that the smaller values of m_{Si} or L require higher separation of E_n from $U(x)$ to reduce errors. The correction term σ_{corr} in (25), explained in the Appendix, helps to minimize this problem. It is recommended to use the

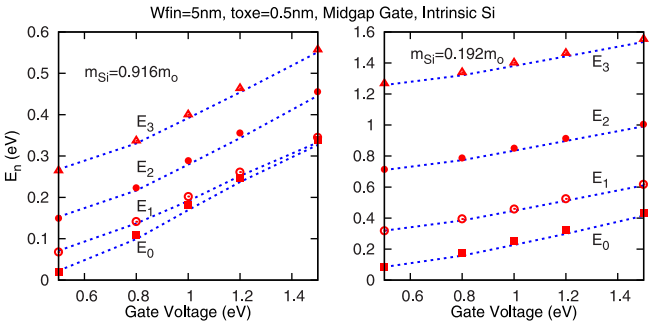

Fig. 7. Energy level (E_0–E_3) dependence on gate voltage, for infinite dielectric barriers. Numerical simulator (symbols) and model (lines) results are shown.

perturbation technique, and not the WKB, for E_n just above U_m for light effective mass (<0.3 m_o) and $W_{\text{fin}} < 5$ nm.

D. Device Simulations

Device simulations for the energy levels without wave function penetration were conducted using SCHRED.

Fig. 7 compares the model-calculated energies with the numerical simulator values, for the case of $W_{\text{fin}} = 5$ nm and $t_{\text{oxe}} = 0.5$ nm, both having midgap gates and intrinsic doping. The model inputs are t_{oxe}, V_{FB}, W_{fin}, and V_g, which are used in (11)–(14) to find γ and U_m. Next, E_n is calculated for the case of infinite dielectric barrier using (22)–(24) for $E_n < U_m$ and (26) for the higher energy levels.

V. Wave Function Penetration

Wave function penetration results in change in the energy level, as well as causes an apparent phase shift in the angle θ defined in (4) and (5) from both sides at the semiconductor–dielectric interface. This is shown in Fig. 8. This is equivalent to stretching the wave function outside $-L$ and $+L$.

Starting with the RR case, the new boundary conditions in (4) can be rewritten as

$$\theta_{\text{pentr,RR}} = \frac{1}{\hbar}\int_{-\Delta x-L}^{L+\Delta x} p_n(x)dx = 2\theta_1 + \frac{1}{\hbar}\int_{-L}^{+L} p_n(x)dx = (n+1)\pi \tag{29}$$

where θ_1 is the phase from each side, which, if the wave function was to continue, would have reached zero, at $L \pm \Delta x$. For the SR case, with $E_n < U_m$, (5) is rewritten as

$$\theta_{\text{pentr,SR}} = \frac{1}{\hbar}\int_{-\Delta x-L}^{-x_0} p_n(x)dx = \theta_1 + \frac{1}{\hbar}\int_{-L}^{-x_0} p_n(x)dx = \left(n+\frac{3}{4}\right)\pi. \tag{30}$$

In order to calculate Δx and θ_1, the potential at $\pm(L-\Delta x)$ can be linearized as straight line, with slope γL. At $x = -L$

$$U_{\text{lin}}(-L) \approx (dU(-L)/dx)\Delta x = \gamma L \Delta x. \tag{31}$$

Thus, at Δx, the linearized momentum $p_n(\Delta x)$ becomes

$$p_n(\Delta x) \approx \sqrt{2m_{\text{Si}}(E_n - \gamma L \Delta x)} \tag{32}$$

while the phase shift inside the dielectric $\theta_1(\Delta x)$ is written as

$$\theta_1 = \sqrt{2m_{\text{Si}}}/\hbar \int_{-\Delta x-L}^{-L} \sqrt{E_n - \gamma L x}dx = (2\sqrt{2m_{\text{Si}}}/(3\hbar\gamma L))\left[E_n^{3/2} - (E_n - \gamma L \Delta x)^{3/2}\right] \tag{33}$$

Note that m_{Si} was used, and not the m_{diel}, since Δx is assumed that to be a virtual extension of the Si potential well. Using (2), the wave function ψ_0 at the barrier interface ($x = -L$), under penetration conditions, can be written as

$$\psi_0 = A_1[p(\Delta x)]^{-1/2}\sin(\theta_1). \tag{34}$$

Differentiating with respect to x

$$d\psi/dx = A_1 p^{-1/2}\cos\theta(d\theta/dx) + A_1(dp^{-1/2}/dx)\sin\theta. \tag{35}$$

For small Δx where θ_1 is small, using $\tan(\theta_1) \sim \theta_1$, and dividing (35) by (34) gives

$$S_{\text{Si0}} = \frac{d\psi_{\text{Si0}}/dx}{\psi_{\text{Si0}}} \approx \frac{\sqrt{2m_{\text{Si}}}}{\hbar}\frac{(E_n - \gamma L\Delta x)^{1/2}}{E_n^{3/2} - (E_n - \gamma L\Delta x)^{3/2}} + \frac{\gamma L}{4}(E_n - \gamma L\Delta x)^{-1} \tag{36}$$

where S_{si0} is the normalized slope for wave function in silicon at the dielectric–semiconductor interface. From dielectric side

$$\frac{d\psi_{\text{diel0}}/dx}{\psi_{\text{diel0}}} = \frac{S_{\text{diel0}}\psi_{\text{diel0}}}{\psi_{\text{diel0}}} = S_{\text{diel0}} = \frac{m_{\text{diel}}}{m_{\text{Si}}}S_{\text{Si0}} \tag{37}$$

where S_{diel0} is equal to $[2\, m_{\text{diel}}(\Phi_B - E_n)]^{1/2}/\hbar$ for rectangular barrier, and can be evaluated as shown in [20] for trapezoidal barriers.

In order to find ΔE, θ_1, and Δx, the following procedure is proposed. This procedure is noniterative, and does not need further corrections. The model developed here assumes a fixed potential profile. It does not consider the effect of penetration on the potential itself.

A. Initial Linear Approximation for θ_1

It is assumed that $U_m = 0$ for the initialization purposes of θ_1

$$\theta_{1,\text{linear}} = \Delta x \frac{(n+1)\pi}{2(L+\Delta x)}. \tag{38}$$

Thus, after ignoring the $dp^{-1/2}/dx$ terms in (35) and using $\sin\theta_1 \sim \theta_1$

$$S_{\text{Si0}} \approx \frac{(n+1)\pi}{2L}\left[\frac{1-\theta_1^2/2}{\theta_1}\right] = \frac{1-(n+1)^2\pi^2\Delta x^2/(8L^2)}{\Delta x}. \tag{39}$$

This is a second-order polynomial in Δx, which can be solved as

$$\Delta x_{\text{linear}} = \frac{4L^2}{(n+1)^2\pi^2}\left[-S_{\text{Si0}} + \sqrt{{S_{\text{Si0}}}^2 + \frac{(n+1)^2\pi^2}{2L^2}}\right]. \tag{40}$$

B. Estimation of Energy Change

In order to avoid iterations and multiple corrections, an initial estimate of energy change is needed. This is done using

$$\frac{dE_{\text{penetr}}}{d\Delta x} = \frac{d\theta_1/d\Delta x}{d\theta_1/dE} = -\frac{\sqrt{2m_{\text{Si}}}}{\hbar}\frac{(E-\gamma L\Delta x)^{1/2}}{d\theta_1/dE} \quad (41)$$

where $d\theta_1/dx$ is the differentiation of (33) with respect to x, $d\theta_1/dE$ is found by differentiating (29) with respect to E, while the integral is solved in an analogous way to (9) and (23), but with integration limits changed. Two cases exist as follows.

1) For the SR case, where $E_n < U_m$, $d\theta/dE$ is directly calculated using (24), after using the value of E_n calculated previously using (7), (22) and (23).
2) For the RR case, where $E_n > U_m$, the integration limits in (9) become from $-L$ to $+L$, as follows:

$$\frac{d\theta_{1\text{penetr,RR}}}{dE} = \frac{1}{2}\frac{\sqrt{m_{\text{Si}}/\gamma}}{\hbar}\ln\left|\frac{L+\sqrt{L^2-a_{\text{RR}}^2}}{-L+\sqrt{L^2-a_{\text{RR}}^2}}\right|$$
$$a_{\text{RR}}^2 = 2(U_m - E_{n,\text{RR}})/\gamma. \quad (42)$$

The new energy level in the case of penetration becomes

$$E_{n,\text{penetr}} = E_n + \Delta E_{\text{penetr}} = E_n + \frac{dE_{\text{penetr}}}{d\Delta x}\Delta x_{n,\text{linear}}. \quad (43)$$

Note that the change in $\Delta E_{n,\text{pentr}}$ is negative. For SR case of $E_n < U_m$, $E_{n,\text{pentr}}$ from (43) should be used once again in (7), (23), and (24) to get two new split levels.

C. Final Calculation of Δx and θ_1

Next, the new energy estimate, together with the initial estimate of Δx_{linear}, is used to refine θ_1 and Δx. The left hand side term in (36) is replaced by $(m_{\text{Si}}/m_{\text{diel}})S_{\text{diel}}$ using (37), followed by a solution of (36) to get a more accurate value of Δx_n. In order to do so, simplifications are made using series expansion of $(1+\varepsilon)^{-1/2} \sim 1+\varepsilon/2+\ldots$, and $(1+\varepsilon)^{-1} \sim 1+\varepsilon+\ldots$ for small $\varepsilon < 1$ [26]. After straightforward rearrangement, a new value of Δx_n can be found by solving a second-order polynomial

$$\Delta x_n = \frac{2E_{n,\text{pentr}}^2}{(\gamma L)^2}\left[-\left(S_{\text{Si,pentr}} - \frac{\gamma L}{4E_{n,\text{pentr}}}\right) + \sqrt{\left(S_{\text{Si,pentr}} - \frac{\gamma L}{4E_{n,\text{pentr}}}\right)^2 + \frac{(\gamma L)^2}{E_{n,\text{pentr}}^2}}\right] \quad (44)$$

where $S_{\text{Si,pentr}}$ is the corrected wave function slope in silicon calculated using the estimate of energy level after penetration, $E_{n,\text{penetr}}^{(0)}$, from (43).

The last step is to calculate θ_1 using (33), based on the new values of $E_{n,\text{pentr}}^{(0)}$ from (43) and Δx_n from (44). The phase angle θ_1 is used to plot the wave function according to (2) and (30).

Table II compares the results for the effect of finite barrier on energy levels using the model equations against the numerical eigenvalue solver. The well width is 5 nm, and $U_m = 0.2$ eV. The effective mass under the barrier m_{Barrier} is assumed to be identical to that of Si in the well, m_{Si}, and assuming a 5 nm barrier width from both sides. The results between parenthesis for $m_{\text{Si}} = 0.192\ m_o$ show the improvement if the infinite barrier energies used as inputs to the penetration model, and are calculated using the perturbation expression in (10).

TABLE II
DEPENDENCE OF ENERGY LEVELS (meV) ON RECTANGULAR BARRIER HEIGHT $m_{\text{Barrier}} = m_{\text{Si}}$, $W_{\text{fin}} = 5$ NM, $U_m = 0.2$ EV

Φ_B (eV)		$m_{\text{Si}} = 0.916\ m_o$				$m_{\text{Si}} = 0.192\ m_o$			
		E_{00}	E_{01}	E_{02}	E_{03}	E_{10}	E_{11}	E_{12}	E_{13}
∞	Num.	181	202	289	401	250	455	843	1389
	Model	179	200	288	400	236 (252)	456	843	1389
3.15	Num.	173	189	273	372	230	386	702	1144
	Model	173	190	270	371	210 (222)	382	687	1116
2	Num.	170	185	268	365	225	370	669	1080
	Model	171	187	265	363	204 (215)	362	644	1027
1	Num.	166	178	260	350	214	337	599	923
	Model	168	181	255	346	193 (201)	320	526	-
0.5	Num.	158	167	248	327	199	292	485	-
	Model	163	173	238	312	178 (182)	237	-	-

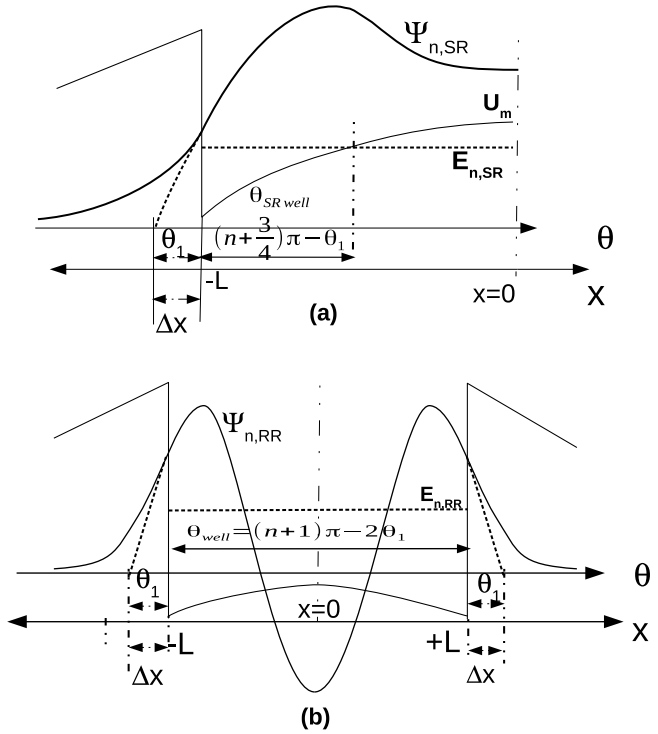

Fig. 8. Analysis of the wavefunction penetration for both SR (top) and RR (bottom) cases. It is assumed that the WKB sin θ term starts from within the dielectric, at an equivalent depth of Δx, where θ is equal 0. (a) $E_n < U_m$. (b) $E_n > U_m$.

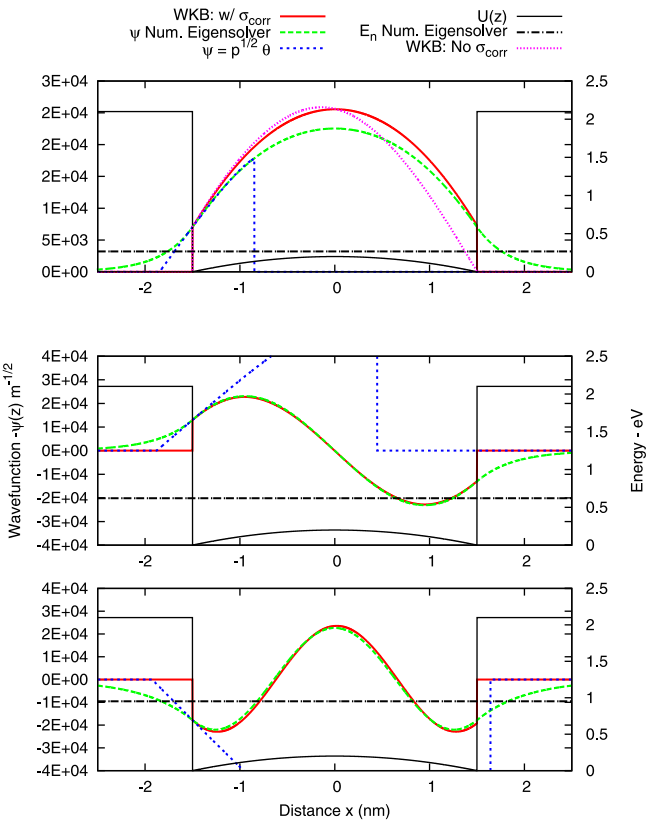

Fig. 9. Wavefunction penetration using the model for the lowest three levels, for $W_{\rm fin} = 3$ nm, $\Phi_B = 2$ eV, $m_{\rm Si} = 0.192$ m_o, and $U_m = 0.2$ eV.

Fig. 9 shows the plots of the wave functions using the analytical integration of (2), after adding the phase angle θ_1, and compares them with the numerical eigenvector solver results. Within the well, the sin $\theta(x)$ term in (34) becomes

$$\psi_n(x) = \frac{1}{\sqrt{p_n(x)}} \sin\left(\frac{1}{\hbar}\int_{-L}^{x} p_n(x)dx + \theta_1 - \sigma_{\rm corr}(x)\right). \tag{45}$$

The integral of $p_n(x)$ in (45) is of standard form $\int(a^2 + x^2)^{1/2}dx$, similar to the RR case in (25). The infinite barrier energies input to the model are the numerical ones, in order to verify the model for θ_1 and Δx, independent of WKB-introduced errors in E_n. The plots show the validity of using θ_1 to represent the wave function penetration, and the simplicity of using the WKB representation to analytically represent the wave function. Also shown is the approximation of $\psi(x = 0)$, using $\sin(\theta_1) \sim \theta_1$ from (34), after inserting (33) to represent θ_1. Energies smaller than U_m require connection rules in order to analytically express the wave function near turning points.

Fig. 9 also shows the importance of using the correction term $\sigma_{\rm corr}(x)$ for phase in the case of light effective mass, and E_n slightly above U_m. The ultrathin $W_{\rm fin}$ of 3 nm also amplifies the change in momentum in the well, adding to WKB errors. For comparison, the first level is shown using the eigenvalue solver for $E_{0,\rm RR}$ without $\sigma_{\rm corr}$.

VI. Conclusion

The WKB quantization rules have been proposed as an alternative method to calculate the energy levels in the SDG FETs. The double well analysis based on WKB approximation can accurately explain the behavior of energy levels and wave function shape in the lowest energy levels.

Results have shown that the assumption of a parabolic potential is valid for the body thicknesses below 10 nm, and can be combined with the WKB rules to arrive to closed form expressions for energies. The proposed method successfully reproduces the energy splitting in the first level(s), in contrast to the perturbation technique, which sometimes fails for these levels. However, the latter method is better for energies very close to the maximum potential maximum at the center of the Si body. Change in energy with finite barrier height, down to 0.5 eV, was successfully calculated using a model based on a phase angle inside the dielectric. The model results were implemented in the device simulation equations to calculate these effects as a function of applied gate voltage, fin width, and equivalent oxide thickness. Numerical eigenvalue/eigenvector solvers were used to verify the basic model, while the self-consistent device simulators were used to verify device results.

Appendix

By including the second-order term in WKB approximation of the phase, the correction term $\sigma_{\rm corr,RR}$ in (25), for $E_n > U_m$, is expressed as [24]

$$\sigma_{\rm corr,RR}(x) = \hbar\int_{-L}^{x}\left[\frac{p''}{4p^2} - \frac{3p'^2}{8p^3}\right]dx. \tag{46}$$

Using (1), the definite integral can be evaluated to yield

$$\sigma_{\rm corr,RR}(x) = w_{\rm corr}(x) - w_{\rm corr}(-L) \tag{47}$$

where $w_{corr}(x)$ is a function defined as

$$w_{\rm corr}(x) = \frac{\hbar\left[x\left(6a_{\rm RR}^2 + x^2\right)\right]}{24\sqrt{\gamma\, m_{\rm Si}}a_{\rm RR}^2\left(a_{\rm RR}^2 + x^2\right)^{1.5}} \tag{48}$$

where $a_{\rm RR}$ is defined in (42).

References

[1] *International Technology Roadmap for Semiconductors (ITRS) 2013 Report*, accessed on Jul. 14, 2016. [Online]. Available: http://www.itrs2.net

[2] Y. Taur, "Analytic solutions of charge and capacitance in symmetric and asymmetric double-gate MOSFETs," *IEEE Trans. Electron Devices*, vol. 48, no. 12, pp. 2861–2869, Dec. 2001.

[3] F. J. García-Sánchez and A. Ortiz-Conde, "A formula for the central potential's maximum magnitude in arbitrarily doped symmetric double-gate MOSFETs," *Solid. State. Electron.*, vol. 76, pp. 112–115, Oct. 2012.

[4] L. Ge and J. G. Fossum, "Analytical modeling of quantization and volume inversion in thin Si-film DG MOSFETs," *IEEE Trans. Electron Devices*, vol. 49, no. 2, pp. 287–294, Feb. 2002.

[5] S. Mudanai, A. Roy, R. Kotlyar, T. Rakshit, and M. Stettler, "Capacitance compact model for ultrathin low-electron-effective-mass materials," *IEEE Trans. Electron Devices*, vol. 58, no. 12, pp. 4204–4211, Dec. 2011.

[6] G. Hiblot, Q. Rafhay, F. Boeuf, and G. Ghibaudo, "Analytical model for the inversion gate capacitance of DG and UTBB MOSFETs at the quantum capacitance limit," *IEEE Trans. Electron Devices*, vol. 62, no. 5, pp. 1375–1382, May 2015.

[7] J. L. Autran, D. Munteanu, O. Tintori, S. Harrison, E. Decarre, and T. Skotnicki, "Quantum-mechanical analytical modeling of threshold voltage in long-channel double-gate MOSFET with symmetric and asymmetric gates," in *Proc. NSTI Nanotech. Conf.*, vol. 2. Boston, MA, USA, Mar. 2004, pp. 163–165.

[8] D. Munteanu, J.-L. Autran, X. Loussier, S. Harrison, R. Cerutti, and T. Skotnicki, "Quantum short-channel compact modelling of drain-current in double-gate MOSFET," *Solid-State Electron.*, vol. 50, no. 4, pp. 680–686, 2006.

[9] F. Chaves, D. Jiménez, and J. Suñé, "Explicit model for direct tunneling current in double-gate MOSFETs through a dielectric stack," *Solid-State Electron.*, vol. 76, pp. 19–24, Oct. 2012.

[10] N. Zettili, *Quantum Mechanics: Concepts and Applications*, 2nd ed. Chichester, U.K.: Wiley, 2009.

[11] E. Merzbacher, *Quantum Mechanics*, 3rd ed. New York, NY, USA: Wiley, 1998.

[12] S. Mohammadi and A. Afzali-Kusha, "An efficient threshold voltage model for ultra thin body double gate/SOI MOSFETs," in *Proc. 10th Int. Conf. Ultimate Integr. Silicon (ULIS)*, Aachen, Germany, 2009, pp. 345–348.

[13] L. D. Landau and E. M. Lifshitz, *Quantum Mechanics*, 3rd ed. New York, NY, USA: Pergamon, 1977, CH. 7.

[14] R. Reuvers, "A flea on Schrödinger's cat—The double well potential in the classical limit," M.S. thesis, Dept. Math. Phys. Astron., Radboud Univ. Nijmegen, Nijmegen, The Netherlands, Aug. 2012. [Online]. Available: http://www.math.ru.nl/~landsman/Robin.pdf

[15] N. P. Landsman and R. Reuvers, "A flea on Schrödinger's cat," *Found. Phys.*, vol. 43, no. 3, pp. 373–407, Mar. 2013.

[16] M. Razavy, *Quantum Theory of Tunneling*. Singapore: World Scientific, 2013.

[17] E. Delabaere and F. Pham, "Unfolding the quartic oscillator," *Ann. Phys.*, vol. 261, no. 2, pp. 180–218, Dec. 1997.

[18] Y. C. Ou, Z. Cao, and Q. Shen, "Formally exact quantization condition for nonrelativistic quantum systems," *J. Chem. Phys.*, vol. 121, no. 17, pp. 8175–8178, 2004.

[19] M. K. Ashraf, A. I. Khan, and A. Haque, "Wave function penetration effects on ballistic drain current in double gate MOSFETs fabricated on (1 0 0) and (1 1 0) silicon surfaces," *Solid-State Electron.*, vol. 53, no. 3, pp. 271–275, Mar. 2009.

[20] A. M. Bayoumi, "Use of WKB approximation for analytical boundary conditions in numerical solution of Schrödinger equation: Application to semiconductor–high-k dielectric interfaces," *Int. J. Numer. Model. Electron. Netw., Devices Fields*, vol. 29, no. 3, pp. 392–406, Jul. 2016.

[21] *DSTEBZ Eigenvalue and DSTEIN Eigenvector Solvers, LAPACK Numerical Package*, accessed on Jul. 14, 2016. [Online]. Available: http://www.netlib.org/lapack/

[22] D. Vasileska *et al.* (2015). *Schred*. [Online]. Available: https://nanohub.org/resources/schred, doi: 10.4231/D34T6F441.

[23] *hksim: High-k MOS Quantum Mechanical Simulator*, accessed on Jul. 14, 2016. [Online]. Available: http://c2eda.net/hksim

[24] H. Friedrich and J. Trost, "Working with WKB waves far from the semiclassical limit," *Phys. Rep.*, vol. 397, no. 6, pp. 359–449, Jul. 2004.

[25] F. Chaves, D. Jiménez, and J. Suñé, "Explicit quantum potential and charge model for double-gate MOSFETs," *Solid. State. Electron.*, vol. 54, no. 5, pp. 530–535, May 2010.

[26] A. Jeffrey, *Handbook of Mathematical Formulas and Integrals*. San Diego, CA, USA: Academic, 1995.

Amr M. Bayoumi (M'89–SM'13) received the B.Sc. degree in computer engineering from Ain Shams University, Cairo, Egypt, in 1988, and the M.Sc. and Ph.D. degrees in electrical engineering from North Carolina State University, in 1992 and 1995, respectively.

He was previously with HP-Labs, Palo Alto. He is currently the Chair of the Electronics and Communications Engineering Department with the Arab Academy for Science and Technology, Cairo. He co-founded the academic project c2eda.net